Development of a 1-MW Target and Beam Monitor for NuMI

Jackson Waters, Lewis University

Mentor: Katsuya Yonehara, Fermilab

August 29, 2018

Abstract

This project consisted of working on the development of two different components in the Neutrinos at the Main Injector (NuMI) facility. The first part of the project focused on finding the optimal configuration of a new graphite target necessary for 1-MW of beam power, while the second part focused on preparing to test a new beam detector design for a radiation robust hadron monitor that is capable of handling a 1-MW beam power. Simulations were performed for finding the target configuration that gave the maximum pion yield. To prepare the beam detector for the beam test, a support structure was designed that could withstand the weight of the detector while keeping it stabilized in its proper position.

Introduction

Fermilab is developing the most powerful neutrino beam in the world looking for physics beyond the Standard Model. LBNF (Long-Baseline Neutrino Facility) will become the state-of-the-art facility for neutrino experiments once it is finished. The current facility producing a wideband neutrino beam is NuMI, which produces neutrinos from the Main Injector (MI) proton beam. The MI proton beam has a momentum of 120 GeV/c, and once this beam is injected into the NuMI beamline, the beam smashes into a graphite target. At this point, scattering occurs, and secondary particles are produced, the most important being charged pions. Charged pions are unstable charged particles that mostly decay into muons and muon neutrinos, which makes the neutrino beam possible. Once the pions are produced from the target, they are directed into a decay pipe by magnetic horns, and the decay pipe itself is almost 700 m long, allowing enough time for pions of various momentums to decay and produce the wanted neutrinos. Right behind the decay pipe, a hadron monitor is setup to monitor any residual charged particles in the beam, and this determines how much the target is deteriorating in a high radiation environment. Figure 1 below shows the layout of the NuMI facility and its associated components.

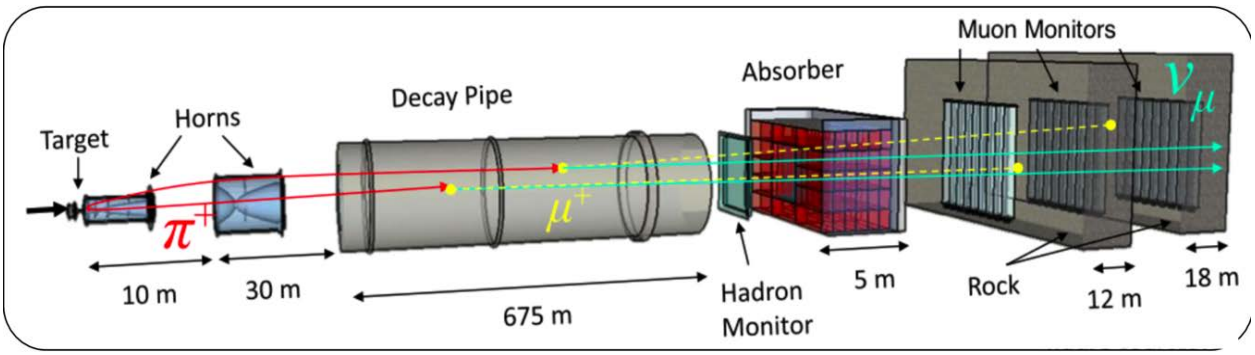

Figure 1: NuMI Layout

Per the accelerator improvement plan at Fermilab, in order to produce a more intense neutrino beam, it will be necessary to increase the power of the primary beam to 1 Mega-Watt (MW). Therefore, the detector components also need to be improved to handle this beam power, and the design of these components may then be implemented into the LBNF design.

The first focus of this project was to upgrade the graphite target producing the charged particles that go on to decay into neutrinos, and make it so that it can handle a 1-MW beam power. For this project, G4Beamline simulations were performed to simulate the target in the NuMI environment with a 120 GeV/c proton beam. The goal of these simulations was to find the target geometry and configuration that gave the highest pion yield.

The second focus of this project was to implement and test a new beam detector that will make up the hadron monitor measuring residual charge in the neutrino beam after going through the decay pipe. The beam test will be performed in the MI-40 Abort Line area, which will allow for a proton beam of the same energy as the proton beam in the NuMI beamline to go through the detector. In this case, the new detector will be a gas filled RF-Cavity, which can measure the residual charged particles in the beam by looking at the permittivity shift in gas becoming ionized by these charged particles. The ionized gas is known as a beam-induced plasma, and the permittivity shift is measured by observing RF signal modulation in the cavity. A beam test has already been performed to test the theory of being able to measure the permittivity shift with a gas filled RF cavity, however, this second beam test will focus on improving the performance of the detector by placing it in a beam with higher intensity. In order to test this detector, a safety assessment providing estimated residual dose levels on the detector needed to be performed. Simulations with FLUKA were performed to measure these residual dose levels on the detector. Also, a new support structure for the beam detector was necessary to place the detector in the correct position with respect to the beam and the other components in the area. Initial stress analysis was performed for this support structure, and stress analysis of the RF cavity itself was performed to verify that it can contain the gas placed into it.

Simulation of the NuMI Target

The current target is 1.2 m in length, and is divided up into 48 graphite pieces, known as fins. Note that we use a standard graphite whose chemical property is given by the Particle Data Group in this simulation. The present NuMI target is the POCO ZXF-4Q, which is 10 % lower mass density than the standard graphite. The length of each fin is 24 mm and the gap between the adjacent fin is 1 mm. Those simplifications do not change our conclusions.

For a target capable of handling a 1-MW beam, a new target design was necessary to handle an increase in beam intensity and a missteered beam occurrence. As the beam hits the target, there is an instantaneous thermal energy generated in the fins. With a higher beam intensity, the beam spot size and the fin width are larger. To prevent the thermal damage to the target due to the fin, a baseline design for the fin width is 9mm with the RMS beam spot size 1.5 mm[1]. A 15-mm-inner bore 1.5-m-long baffle is located in front of the target to protect the 18-mm-inner bore horn conductor, which is located downstream of the target. An 18-mm-diameter winged fin is added in the target to reduce the density of missteered beam at the upstream decay pipe window.

However, the winged fin will also reduce a neutrino flux in a normal operation because the produced pions in the fins are captured in the winged part. The location of winged fins and the number of winged fins are a variable parameter to minimize the capture rate while the diameter is fixed. Figures 2 and 3 display the engineering drawings for a 1-MW fin and a winged fin.

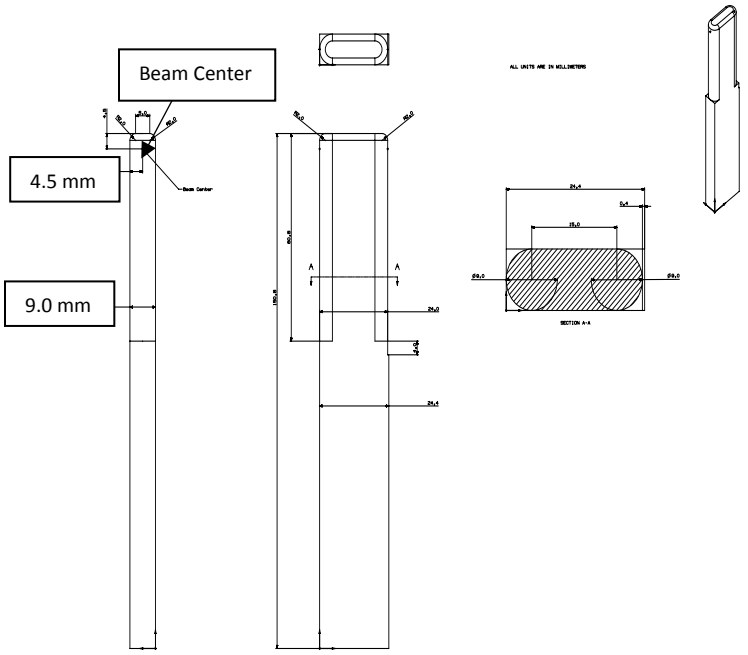

Figure 2: 1-MW Fin Engineering Drawing

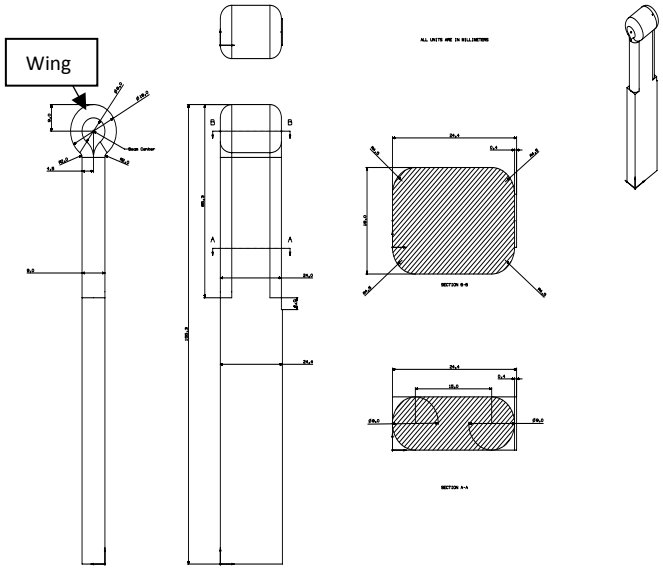

Figure 3: Winged Fin Engineering Drawing

We use G4Beamline for the target simulation study. The goal is maximizing the pion yield which is the number of pions normalized by the number of incident protons. The simulated pions are filtered by the total momentum above 2 GeV/c when we analyze the result. First, we tested the simulation code by varying the number of test particles and looking at the statistical fluctuation on the pion yield. The winged fin counts and the fin width dependences were studied. A simulation picture in Figure 4 shows a general picture of what winged fins in the downstream section of the target would look like.

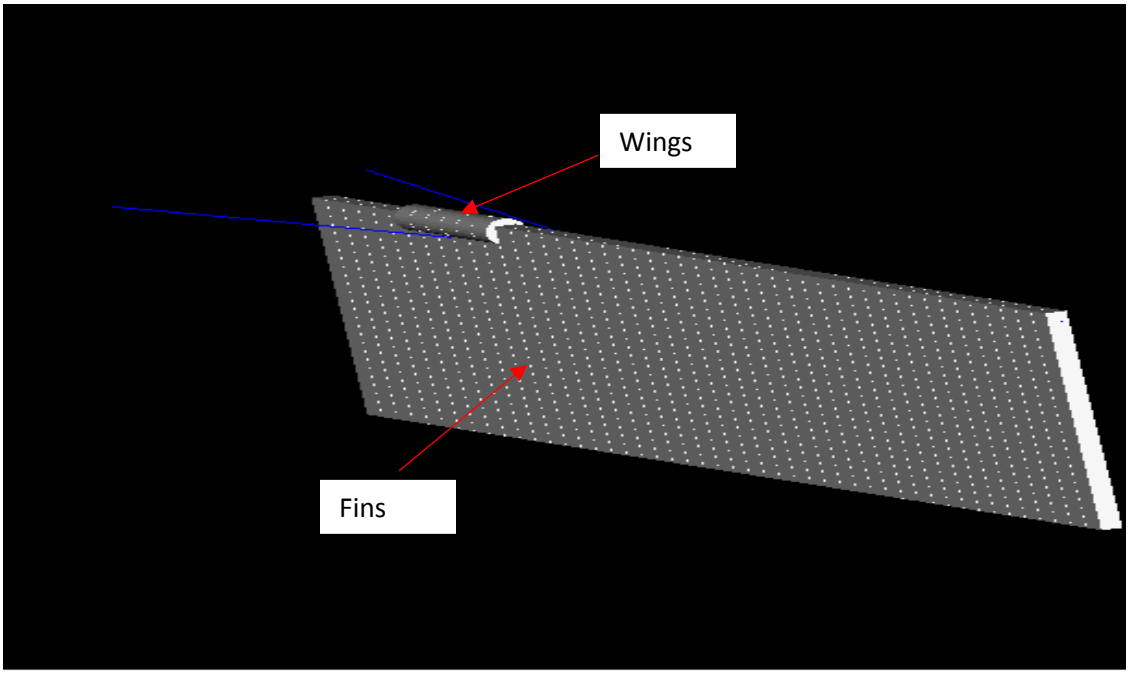

Figure 4: Simulation of Target with Downstream Winged Fins

Figure 5 shows the pion yield as a function of the incoming proton intensity. The number of incoming protons was varied from 1000 to 20,000. The pion yield is found by measuring the number of both signed pions produced (Npion) at the downstream end of the target and then dividing that number by the number of incoming protons (Nproton). The expectation for this was to find the point at which the variance in the pion yield starts to become stable at a 1 % level based on the incoming particle intensity.

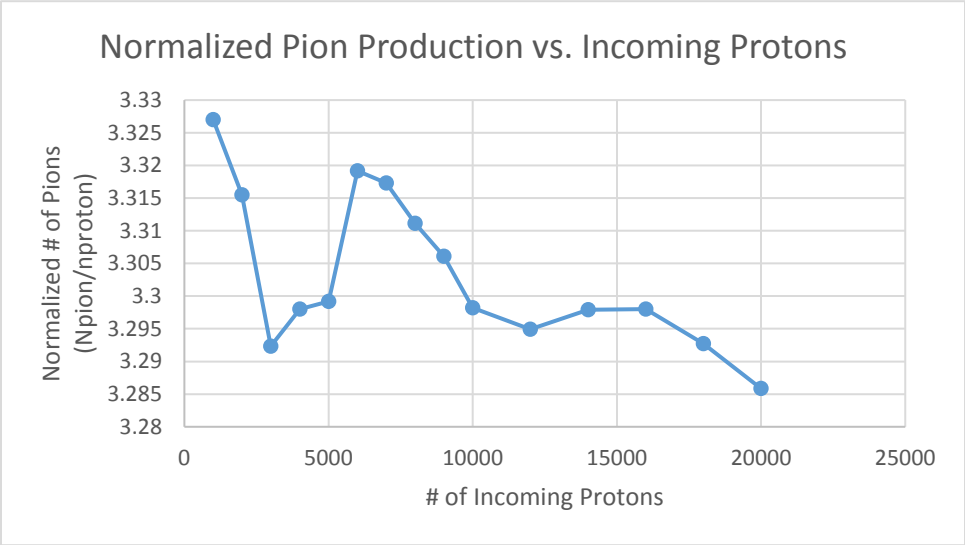

Figure 5: Normalized Pion Yield as a Function of Incoming Protons

Based on this data, the point at which the variance level starts to decrease the most is when the number of incident protons is 10,000. This data shows large oscillations in pion yield for lower proton beam intensities, and these oscillations get smaller as the number of incident protons increases. The percent difference in pion yield at each of these points allows for the variance level to be measured, and once the variance level is 1 % for the number of pions produced, this is the optimal number of incident protons to use for the rest of the simulations. Therefore, once the number of incoming protons gets to 10,000, the large oscillations stabilize and the pion yield is at its most effective point.

The next simulation performed was the inclusion of winged fins at the front (upstream) and back (downstream) ends of the target separately. Therefore, not all of the fins in the target were regular fins, and the number of regular fins and winged fins added up to 48 fins depending on the number of winged fins implemented. These simulations were done to look at the pion yield as a function of the number of winged fins at either the upstream or downstream end of the target. For the upstream section of target, the winged fins started at z = 0 mm, and the number of winged fins was varied from 2 fins up to 10 fins in increments of 2 winged fins. For the downstream end of the target, the winged fins would start at z = 900 mm and the same changes were made as with the winged fins at z = 0 mm.

Figure 6 shows the data for simulations of the target with either upstream or downstream winged fins. This plot is the estimated pion yield (only positive charged pions are used in the rest of simulations) as a function of the number of either upstream or downstream winged fins placed in the target.

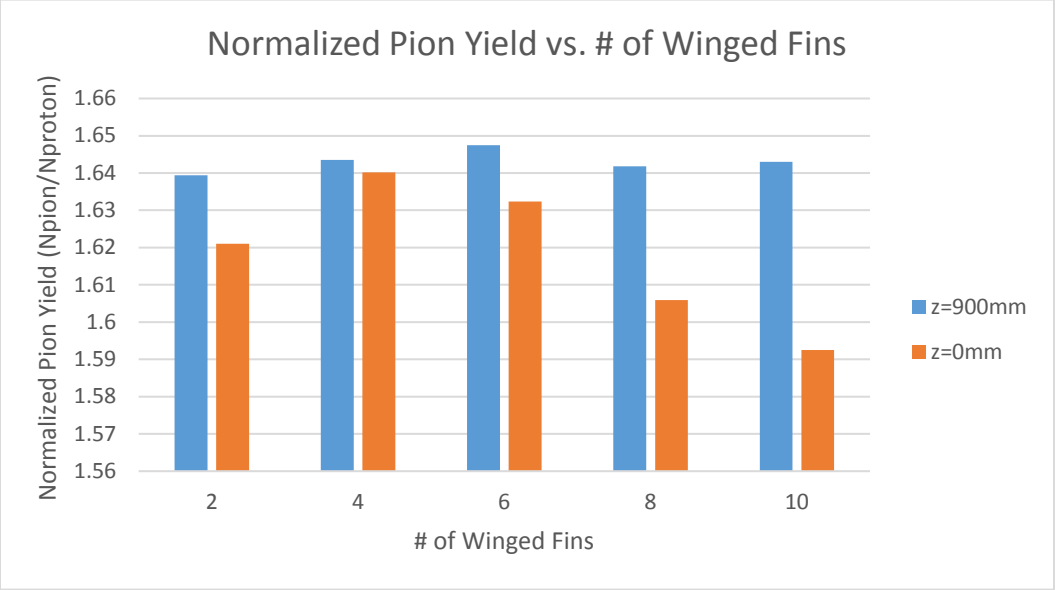

Figure 6: Simulated Pion Yield as a Function of the Number of Wings at Both z = 0 mm and z = 900 mm

This data demonstrates that the optimal number of upstream winged fins placed in the target is 4, and the optimal number of downstream winged fins is 6. Also, a comparison can be made between using either upstream or downstream winged fins in the target. Based on this data, there is a higher pion yield for when downstream winged fins are placed in the target (z = 900 mm). Additionally, with this target configuration, for each number of winged fins, the downstream winged fins seemed to show very similar pion yields that are all higher than that for upstream winged fins. One hypothesis for this is that the beam diverges as it goes through the target material. This means the beam spot size is growing and getting larger as it moves through the target. Therefore, at the downstream end of the target, the beam spot size is larger than it was upstream. With a larger beam spot size downstream, pions produced within the target don't have to travel through as much target material to escape than they would at the upstream end of the target. This explains why more pions can be produced with winged fins at the downstream end of the target than the upstream end because more pions are being absorbed in the upstream winged fins.

The baseline fin width in the target is 9 mm, so in the simulation, by varying the fin width from 8-10 mm in 0.2 mm increments, the optimal fin width can then be found. The fin width was varied for a target configuration with just regular fins, with winged fins at the upstream end of the target, and with wings at the downstream end of the target as well. When the winged fins were implemented, the radius of the wing was kept constant while the fin width was varied. For fin width variance of the upstream winged fin target configuration, only the configuration with 4 upstream winged fins was used in this simulation, and for the fin width variance of the downstream winged fin configuration, only the configuration with 6 downstream winged fins was used.

Figure 7 below illustrates the pion yield as a function of width for the three various beam designs (no wing, winged fins at z = 0 mm, winged fins at z = 900 mm).

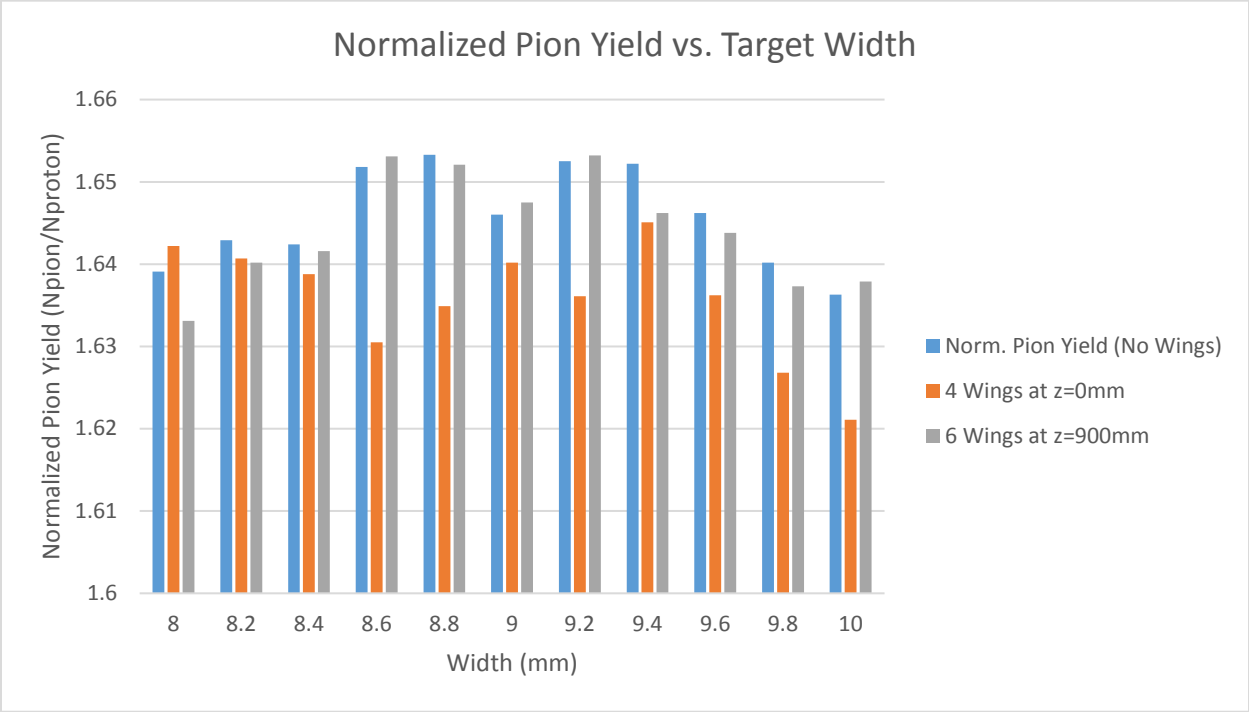

Figure 7: Normalized Pion Yield vs. Fin Width

Based on this data, for the target design with winged fins at the upstream end of the target (z = 0 mm), the highest pion yield is at 9.4 mm. Also, for the target design consisting of no winged fins and for winged fins at the downstream end of the target (z = 900 mm), the highest pion yield is at an 8.8 mm width for no winged fins in the target, and the highest pion yield for downstream winged fins in the target is when the width is 9.2 mm. However, these values are within a 1 % deviation level of each other, and since the simulation variance level is also on a 1 % level, the difference between the pion yield from 8.8 mm to 9.4 mm is due to variance in the simulation. Based on the result, we have ordered a 9-mm-thick POCO graphite plate.

To look at the variance levels seen for the optimal target configuration of 6 winged fins at the downstream end of the target, another simulation was run to vary the random number seed of the simulation, known as the firstEvent number[2]. This is again looking at how much the pion yield varies for the same target configuration, so no trend should be seen in analysis taken from this simulation. The pion yield as a function of the firstEvent number is seen in Figure 8 below.

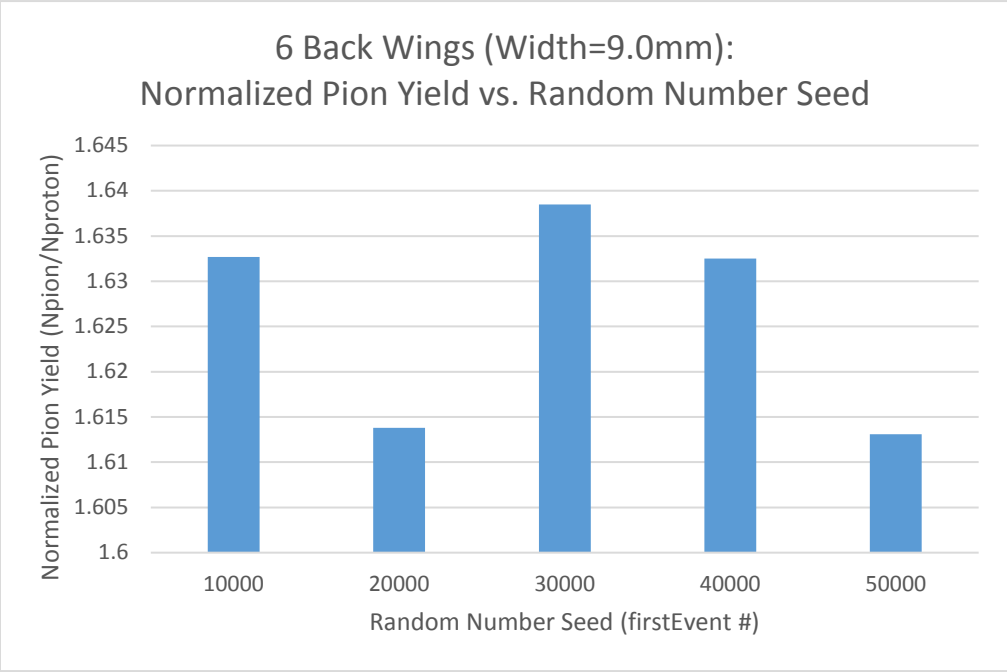

Figure 8: Simulated Pion Yield as a Function of Random Number Seed

The data here shows no trend as expected, and the variance level is on the order of 1 %. This ensures that the simulation variance is low enough to see accurate results from the simulations being performed for winged fins. Also, since some of the results have shown very close numbers for pion yield in relation to the target configuration, if the variance is on the order of 1 %, then this verifies the simulation is the result of the variance.

Furthermore, based on neutrino yield results in a full NuMI beamline simulation performed by the NOvA target simulation group, a 40 fin graphite target was shown to give the highest neutrino yield. Therefore, simulations were performed in G4Beamline to observe the pion yield with a 40 fin graphite target configuration with winged fins placed again either at the upstream or downstream positions. The target length in this case is shortened to 1.0 m, and its length is reduced by taking 8 fins off of the front end of the target. Figure 9 shows the results for the normalized pion yield as a function of winged fins at the upstream (z = 200 mm) and downstream (z = 1000 mm or z = 1100 mm) positions. These positions were each shifted by 200 mm downstream on the target because 200 mm was taken off of the front of the target.

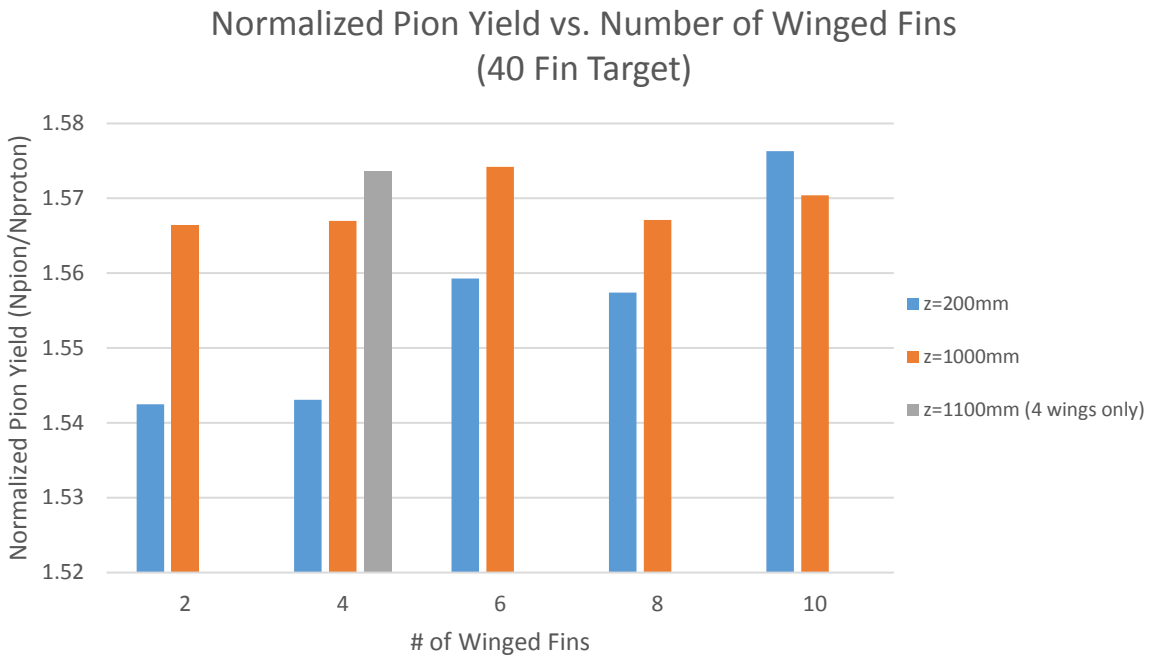

Figure 9: Simulated Pion Yield as a Function of Winged Fins at z = 200 mm (upstream), z = 1000 mm, and z = 1100 mm (downstream) for a 40 Fin Target

These results from Figure 9 show that the highest pion yield was seen for 10 winged fins at the upstream location. Also, the next two highest configurations were for 4 winged fins at z = 1100 mm, and 6 winged fins at z = 1000 mm. All three of these pion yields were within a 1 % difference of each other, and many of these configurations produced yields very close to each other.

Moreover, with this 40 fin target, beam scans were performed to ensure that the expected proton beam intensity profile would be seen at the hadron monitor in the simulation. G4Beamline simulations were used to look at the proton intensity at the location of the hadron monitor based on the horizontal or x position of the beam. The expected profile of proton intensity getting to the hadron monitor 700 m downstream is to see a high proton intensity for when the beam horizontal position is outside of the target width with a minimum intensity for when the beam is at the center of the target. When a baffle (coaxial cylindrical structure) is placed in front of the target, the beam intensity is expected to rise up initially as it goes outside of the target and then go back down to a minimum as it starts to hit the baffle. The baffle is included because it is included in the NuMI beamline area for beam scraping, and this will give a more realistic profile of the beam intensity during the simulation. Also, the target configuration was varied from just a 40 fin regular target to a 40 fin target with 4 front winged fins (radius = 9.0 mm). This was done to see if there was any difference between the proton intensity profile for the two configurations. For these simulation runs, the beam position was varied from x = -10 to 10 mm from the origin, and the virtual detector (diameter = 1 m.) was placed 700 m downstream from the end of the target.

In this case, the virtual detector will act as the hadron monitor detecting the proton beam passing through it. Figure 10 below shows the results of these beam scans with the baffle included.

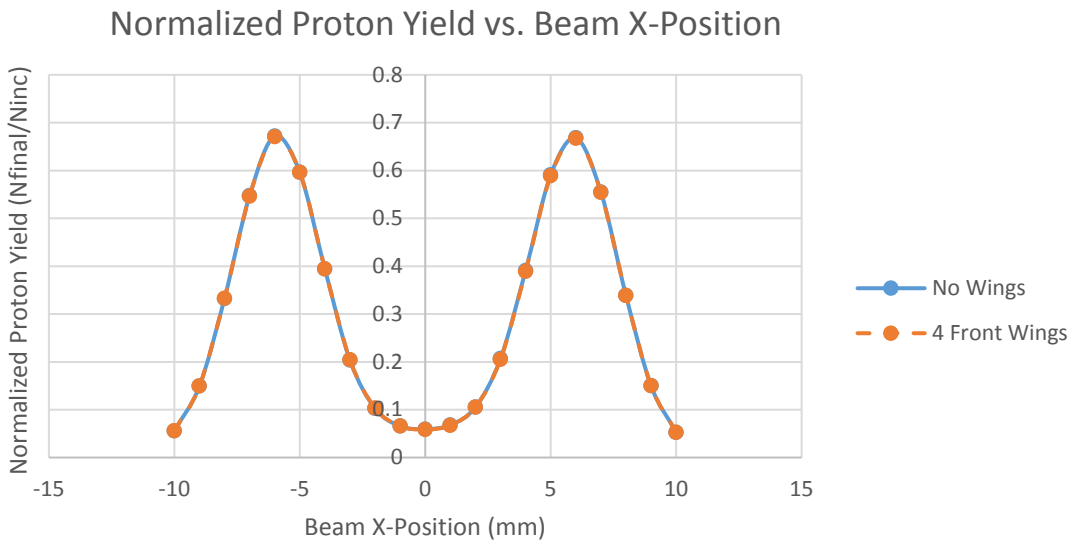

Figure 10: Simulated Normalized Proton at the Hadron Monitor Position as a Function of Beam Horizontal (X) Position

Based on these results, the simulated normalized proton as a function of the horizontal beam position shows the expected profile for the regular finned target, and with 4 front wings, the profile does not really change and has a very close proton transmission efficiency to that of the regular target. With the baffle included, the proton yield does decrease when going past x = ±7 mm, as this is about the inner radius (7.5 mm) of the baffle shell. Therefore, with both of these profiles being seen for a target with 4 front wings and no wings, we should be able to know the center of the target and baffle with the winged fin configuration because high momentum protons are still going through the wings when they are directly being hit by the initial beam. Note that, according to the analytical calculation, the beam is approximately thirty times enlarged by passing through four winged fins. The beam radius is about 5 cm, which is still much smaller than the size of virtual detector (1 m diameter).

Overall, G4Beamline simulations are a useful tool for simulating the NuMI target, and it allows for the generation of preliminary results that can be guide us in the right direction for proper target configuration. Maximizing the pion yield was the goal for looking at the correct target configuration. Based on those results, a downstream winged fin target configuration provides an alternative option to upstream winged fins. Depending on the number of winged fins that will be used, in most of the cases, except for 10 winged fins upstream, the downstream winged fin configuration gave the highest pion yield. Therefore, to verify that this configuration truly can work, a neutrino yield simulation for the full NuMI beamline needs to be performed in order to confirm that maximizing the pion yield in G4Beamline simulations provide accurate results. After the Lee Teng program 2018 was done, we talked with Leonidas Soplin who carried out the full neutrino yield simulation. His latest result shows that the downstream winged fin option

shows better neutrino yield at a low energy region. The NOvA physics group will approve the final target design in September 2018, and we will start making the 1-MW capable target from October 2018.

Preparing a 1-MW Beam Detector for a Beam Test

A new hadron monitor needs to be developed for a high intense beam, with higher levels of radiation. This hadron monitor will consist of multiple beam detectors that can take into account beam position variance and the beam profile at different positions along the beamline. The design of this beam detector is proposed to be more radiation robust as it consists of a gas-filled RF cavity. It is a 2.45 GHz pillbox that will be filled with up to 2 atm of air[1]. The cavity body is made out of an aluminum alloy material known as Al 6061-T6. From this, one can easily monitor the permittivity shift in the gas becoming ionized, known as beam induced plasma, in the cavity as charged particles go through it. A first beam test was performed in Spring 2018 to verify the theory of the new design, ensuring that it will measure the permittivity shift in this beam induced plasma[3]. However, the beam intensity was not high enough to see comparable results to that of the NuMI beam. Therefore, a second beam test is proposed to be done with a high intense beam going through the detector. This test will allow for improved performance of the detector when being implemented into a beam similar to NuMI. The test area that will be utilized for this second beam test is the MI-40 abort line, which will have protons from the Main Injector going through the detector. A proton energy ranging from 20-120 GeV will go through the detector with a high intensity proton beam. Figure 11 shows the aluminum alloy body of the cavity that will be used for this beam test.

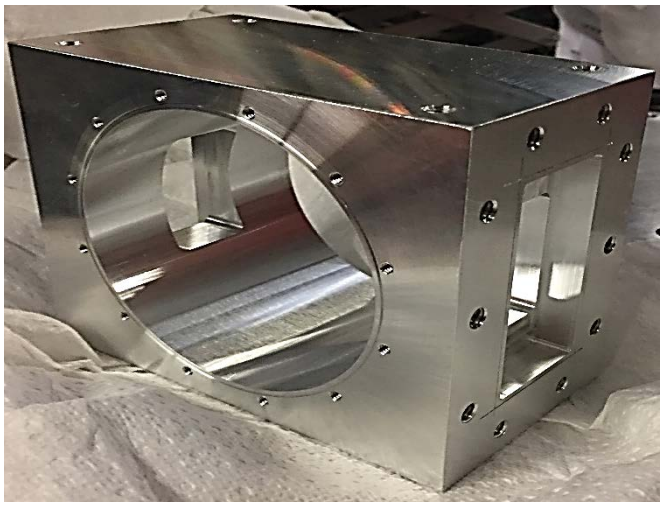

Figure 11: Al 6061-T6 Cavity Body

For this beam test, it was necessary to perform a safety assessment to look at equivalent dose rate levels that would be received from the beam detector with this beam going through it. In order to do this, simulations with a Monte Carlo based simulation package, known as FLUKA, were performed to show an estimate of these equivalent dose rate levels. These simulations were

performed with a beam intensity of 10^{12} p/s, with a beam transverse size of 0.02 cm to evaluate a residual dose for the MI-40 abort line beam, and a beam transverse size of 9.36 cm for the NuMI beam. These simulation results also showed how radiation robust the beam detector is compared to that of a beam detector made of an iron material. The detector itself was centered at the origin, with its longitudinal size ranging from z = -3.81 cm to z = 3.81 cm, while its radial position went out to about R = 4.68 cm.

Figures 12 and 13 below display the equivalent dose received from both the aluminum and iron based RF cavity detectors in a 120 GeV/c proton beam with the small transverse size of 0.02 cm (X(FWHM) = Y(FWHM) = 0.02 cm). The plots show the equivalent dose rate as a function of radial position and longitudinal position in centimeters.

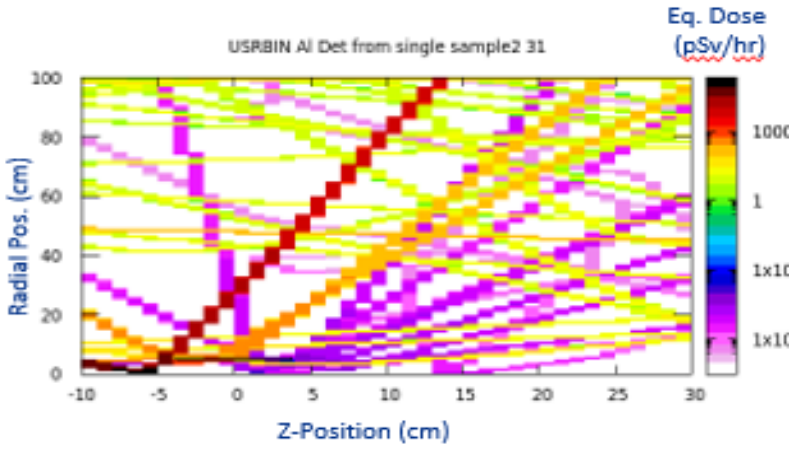

Figure 12: Equivalent Dose Rate Received in One Hour (Al, Small Beam Size)

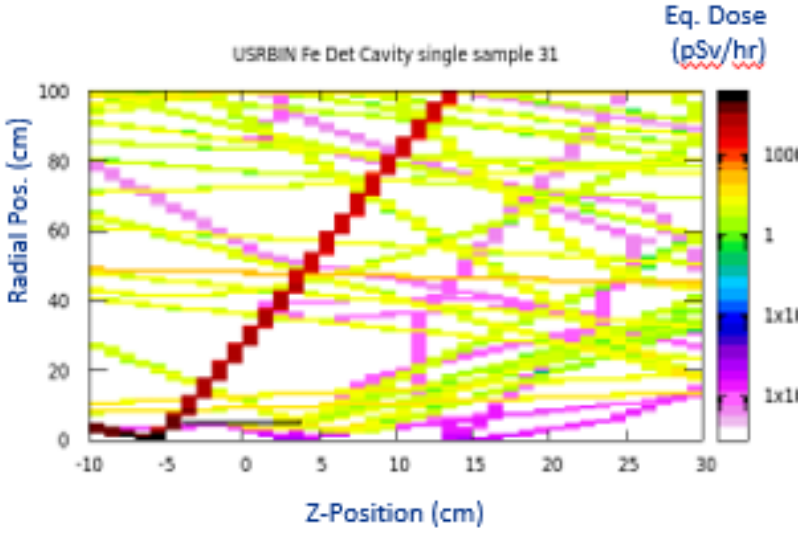

Figure 13: Equivalent Dose Rate Received in One Hour (Fe, Small Beam Size)

These results show that the iron detector gives off higher levels of radiation in one hour than the aluminum based RF cavity detector. The green levels of radiation are more prominent with iron, and these are much higher than the purple levels, which are seen a lot more for the aluminum detector.

Next, simulations were run with a NuMI beam transverse size of 9.36 cm for the aluminum based detector. Figure 14 below demonstrates the equivalent dose rate received in one second of beam from the detector.

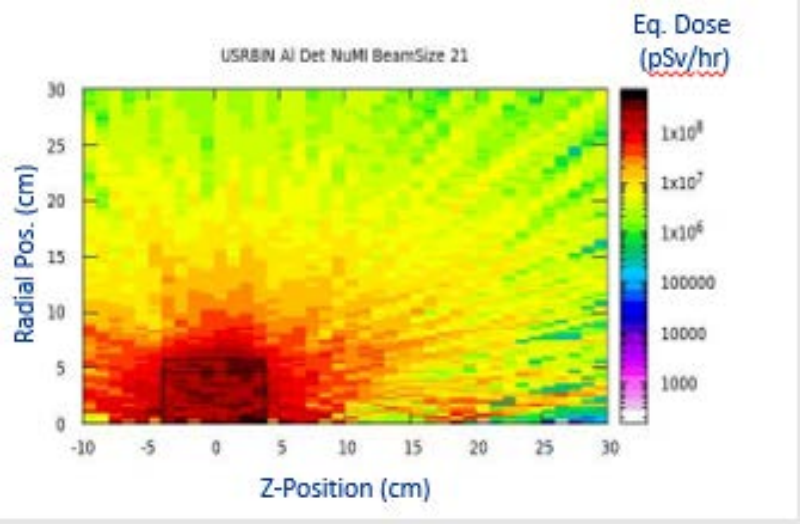

Figure 14: Equivalent Dose Rate Received in One Second (Al, NuMI Beam Size)

The equivalent dose rates seen in Figure 13 are much higher because with a large transverse beam size, the beam is actually hitting the detector shell, producing more ionizing radiation. These higher levels of radiation are expected for the NuMI beam, and actually, since this data only shows the equivalent dose rate received in a second of beam, then the after a year of accumulated beam from NuMI, the equivalent dose rate would actually be on the order of 10^6 times larger than these results.

Additionally, the equivalent dose rates were scanned after the beam was turned off for one second, one hour, ten hours, and then one-hundred hours. These times are known as the cooling time of the detector, as it is the time the detector has not been taking any beam. Therefore, radiation levels will decrease over time, allowing the detector to “cool-off”.

Figure 15 illustrates the equivalent dose rate as a function of the cooling time.

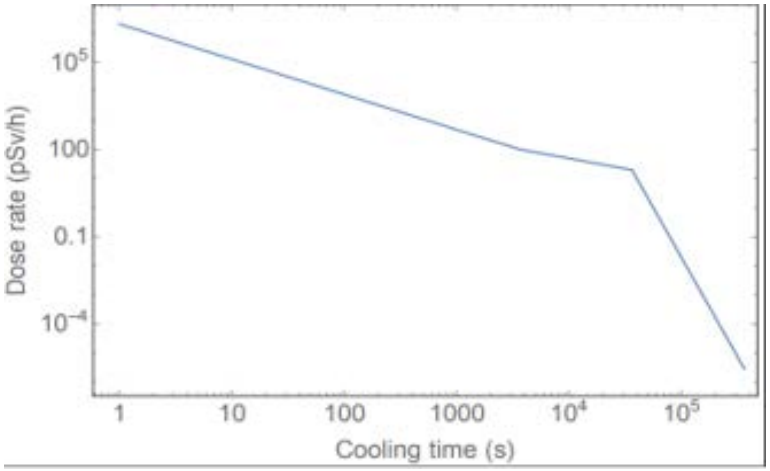

Figure 15: Equivalent Dose Rate as a Function of Cooling Time

As expected, the plot in Figure 15 above shows that as time goes on without beam, the dose rates go down as well. The drop in dose rate after 10^4 seconds looks real. We saw this behavior in the MARS dose analysis as well. Further study will be made for the radiation safety assessment.

The next step in preparing for the beam test was designing a support structure that could support the weight of the beam detector, while also not interfering with any components of the MI-40 abort line that are currently present. Figure 16 shows a real picture of what the setup in the MI-40 abort line area currently looks like.

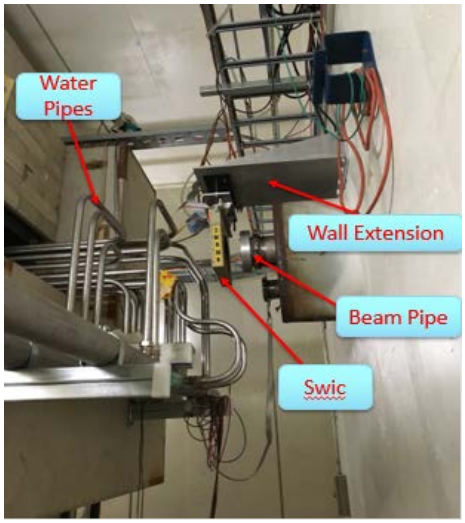

Figure 16: Current MI-40 Abort Line Setup

In order to implement the beam detector into this current area, the current beam monitor in the area, known as the swic (pictured above), needed to be shifted upstream towards the beam pipe. This allows for the beam detector to be fully attached to the wall extension with enough support. Thus, the swic needed to be moved 2.5” upstream, and it could still be fully supported as well, while the new beam detector is placed behind it.

For the support structure design, to implement the beam detector into the area in the proper position, it would be necessary to have a support structure that could allow for the detector to shift in each direction. Therefore, a support structure with an intermediate plate design with adjusters would be implemented. For attaching to the support structure, a system of clamps would be implemented on both sides of the wall extension, with a plate attached below the wall extension. This allows for threaded rods to extend from the top plate down to the intermediate plate. Another set of threaded rods would then extend from the intermediate plate attaching to the beam detector. These threaded rods are adjustable as well, meaning the detector could be adjusted vertically if necessary. A diagram of a new MI-40 layout with the beam detector and its designed support structure is shown in Figure 17.

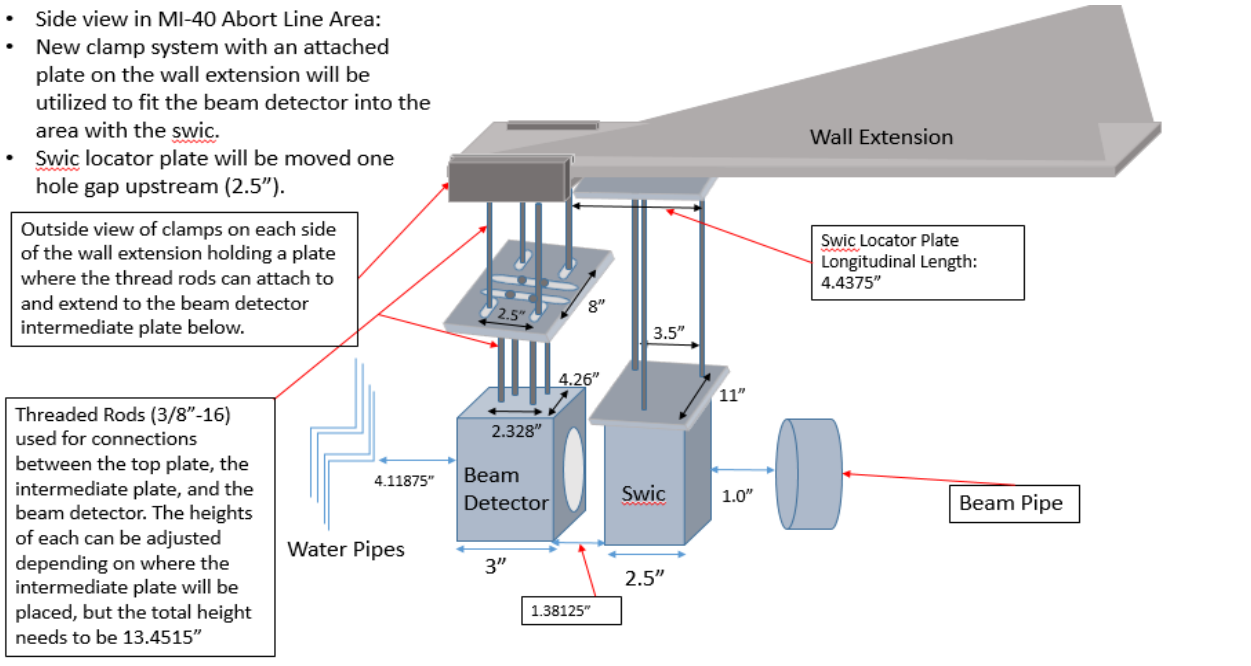

Figure 17: New Side View Layout of MI-40 Abort Line Area with Beam Detector Included

The Main Injector Engineering group has accepted this designed support structure, however stress analysis needed to be performed to ensure that the support structure and the wall extension can hold the beam detector.

Support Structure Stress Analysis Calculations:

Stress analysis calculations were performed for the intermediate plate of the support structure, since this is what the detector directly attaches to. From these calculations, the same parameters can then be implemented for that of the top plate and the clamps as well.

The two necessary calculations to be performed are for finding the maximum stress on the plate and the maximum deflection of the plate under stress. The stress felt by the plate is directly related to the force being applied to the plate from the weight of the attached beam detector. The deflection of the plate is the distance the plate will bend when an external force is placed on it. The diagram in Figure 18 below displays how to visualize a concentrated central force felt on the plate, and that it is concentrated over an area with a diameter of 2e in the middle of the plate.

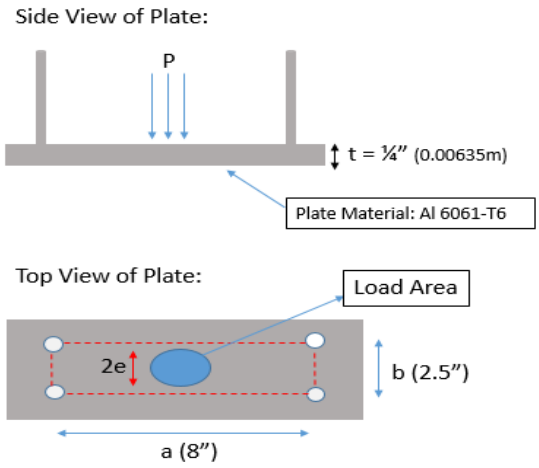

Figure 18: Diagram of Concentrated Force (Load) Felt by the Plate

The set of equations below show the maximum stress felt by the plate at the center, the maximum stress at the edge of the plate, and the maximum deflection of the plate. These were used for an edge clamped rectangular plate with the load concentrated at the center (as shown in Figure 17)[4]:

$$\sigma_{mc}(\max stress\ at\ center) = \frac{1.5P}{\pi t^2}\left((1+\nu)\ln\left(\frac{2b}{\pi e}\right)+k_3\right) \quad (1)$$

$$\sigma_m\ (\max stress\ at\ middle\ of\ edge\ a) = k_2\left(\frac{P}{t^2}\right) \quad (2)$$

$$y_m\ (\max deflection) = k_1\left(\frac{Pb}{Et^3}\right) \quad (3)$$

The list of variables for these equations is shown below:

t = Plate Thickness (m) = ¼" = 0.00635m.

P = Concentrated Force (load) (N) = 49.05N.

e = Load Area Radius (m)

a: Major Length of Rectangular Plate (m) = 8" = 0.2032m.

b: Minor Length of Rectangular Plate (m) = 2.5" = 0.0635m.

$\nu = Poisson's\ Ratio = 0.33\ (for\ Al\ 6061 - T6)$

E = Young's Modulus = 68.9 GPa (for Al 6061-T6)

$\frac{a}{b} = 3.2 \ \rightarrow \ k_1 = 0.0791,\ k_2 = 1.008,\ k_3 = 0.067$

Since there is an area at which the concentrated load acts upon, and the points of attachment to the detector are the 4 short 3/8" (0.375 in.) thread rods, the diameter was calculated based on the hole widths.

$$2e = 4(0.375) \rightarrow e = 0.75" = 0.01905m$$

After plugging the values of these parameters into the three equations, these were the calculated values:

$$\sigma_{mc} = \frac{1.5\ (49.05)}{\pi(0.00635)^2}\left((1 + 0.33)\ln\left(\frac{2(0.0635)}{\pi(0.01905)}\right) + 0.067\right) \approx 620{,}116.9\ Pa$$

$$\sigma_m = \ (1.008)\left(\frac{49.05}{0.00635^2}\right) \ \approx \ 136{,}242\ Pa$$

$$y_m\ (\max deflection) = \ (0.0791)\left(\frac{(49.05)(0.0635)}{(68.9 \times 10^9)(0.00635)^3}\right) \approx \ 3.28 \times 10^{-8} m$$

These equations were calculated assuming that the concentrated center beam load area was the area of a circle with a radius that was the sum of the 4 different threaded rod hole radii for the beam detector attachment. Now if the load area only has a diameter that is equal to one quarter inch hole diameter, then the value of e changes.

$$e = 0.125" = 0.003175m.$$

$$\sigma_{mc} = \frac{1.5\ (49.05)}{\pi(0.00635)^2}\left((1 + 0.33)\ln\left(\frac{2(0.0635)}{\pi(0.003175)}\right) + 0.067\right) \approx 2{,}004{,}206\ Pa = 2.004\ MPa$$

The maximum stress at the edge of the plate and the maximum deflection stay the same, as the load radius only affects the maximum stress at the center of the plate based on these equations. The yield point of the aluminum alloy Al 6061-T6 is 276 MPa, which means this is the maximum stress that this material can handle while not undergoing any permanent deformation in its shape. This is the stress point at which the material will start to bend and cannot be brought back to its original shape after bending. However, for this aluminum rectangular plate, the maximum stress is well below the yield point even if the area was concentrated at the same width as one threaded rod hole. Therefore, the intermediate plate can hold up the detector without surpassing its yield point and without too much deflection causing a shift in the detector vertical position.

Based on these calculations, the next step would be to use them to calculate the amount of bending and stress on the top plate and clamping system. Engineering stress analysis will also be

done to ensure that the wall extension can handle the swic and the new beam detector with its support structure being implemented as well. This will confirm that the support structure can be utilized with the new beam detector, and then an engineering design will be sent to a machine shop to make the components of the support structure.

Stress Analysis on RF Cavity Based Detector

In order to verify that the RF Cavity can withstand a pressure of 2 atm (30 psi) from the gas inside, stress analysis calculations were performed. This analysis was based on a previous analysis done on a cylindrical test vessel[5]. It was used to calculate the minimum required thickness of the cylindrical shell, the minimum required thickness of flat circular heads, and the plug shear stress. The cylindrical shell is the body of the cavity, while the flat circular heads are basically the two disks that will cover the circular openings of the cylindrical shell. The plug shear stress is the amount of stress felt by the screws attaching these flat circular heads to the cylindrical shell when an internal pressure is applied from 2 atm of gas inside the shell. Each of these calculated values were then compared to that of the actual measured values to ensure they meet the necessary requirements. Equations from the previous analysis are used with modifications made for the new cavity:

- Cylindrical Shell Minimum Thickness[5]:
  - $t = \frac{PR}{SE - 0.6P}$ (4)
    - t=minimum thickness of shell
    - R=inside radius of shell=1.8425”
    - P=internal pressure=30 psig
    - S=allowable stress=21,000 psi for Al 6061-T6
    - E=Weld Efficiency=1
  - $t = \frac{(30)(1.8425)}{((21{,}000)(1) - (0.6)(30))} = 0.00263"$

The actual thickness of the cavity is 0.394” which is well above the minimum thickness requirement. Therefore, the cavity, with this thickness, can withstand a pressure of 2 atm.

- Minimum Flat Head Thickness[5]:
  - $t = d\left(\frac{CP}{SE} + 1.9Wh_g/SEd^3\right)^{1/2}$ (5)
    - t = thickness of flat head
    - C = factor for attachment = 0.25
    - P = pressure = 30 psig

- S = allowable stress = 21,000 psi
- E = weld efficiency = 1 (no welds)
- d = diameter of head = 10.5”
- W = total bolt load (unneeded since $h_g = 0$)
- h_g = gasket moment arm = 0 (gasket symmetry about bolt)

– $t = 4.49(0.25(30)/21{,}000)^{1/2} = 0.0849"$

- For a flat head not producing edge moments[5]:

– $t = d\sqrt{\frac{CP}{SE}}$ (6)

– $t = 4.49(0.25(30)/21000)^{1/2} = 0.0849"$

The actual flat head thickness is 0.394”, which is also well above the minimum thickness requirement and can handle 2 atm of gas. Therefore, the thickness of the beam detector has been verified and no changes need to be made.

Next, the plug shear stress is calculated. Again, plug shear stress is the uniform shear stress at the circumference of a disk under operating pressure[5]:

- Plug Shear Stress:

– $\tau = \frac{PA}{2\pi rt}$ (7)

- t = thickness of disk = 0.08”
- A = surface area of disk = 0.122 in^2
- P = operating pressure = 30 psi
- r = radius of hole = 0.19685”

– $\tau = \frac{30(0.122)}{2\,(3.14)(0.19685)\,(0.08)} = 37\ psi.$

The maximum plug shear stress that the aluminum alloy material, Al 6061-T6 can handle is 6124 psi. Thus, the plug shear stress that will be felt by the screws attaching the flat heads to the cylindrical shell is well below the maximum.

Based on these calculations, the new RF-Cavity based detector can be filled with 2 atm of gas, as it meets all of the requirements for thickness and plug shear stress.

Conclusions and Future Work

Overall, this project focused on two parts of the NuMI beamline components to be improved for 1-MW of beam power, the target and the hadron monitor. The goal for the target was to run

simulations with different target configurations to find the maximum pion yield. We confirmed the fin width 9 mm is reasonable in this study. We have ordered a 9-mm-thick POCO plate. Utilizing a winged fin configuration at either an upstream or downstream target location, the pion yield was then observed as a function of the number of winged fins at either of these locations. It was found that the downstream winged fin target configuration gave very high pion yields, while the upstream target configuration also gave a high pion yield for 10 winged fins in a 40 fin target. The NOvA simulation group confirmed our conclusion in their neutrino flux simulation studies. The NOvA physics group will approve the final target design in September 2018 and we will start making a new target. Furthermore, for the hadron monitor, a second beam test needs to be performed on the beam detector making up the hadron monitor. Radiation simulations were performed to ensure the aluminum alloy material was radiation robust and to see how high of an equivalent dose rate would be received with a beam transverse size that is the same as the NuMI beam transverse size. Also, a support structure was designed for the beam detector to be implemented into the beam test area, and initial stress analysis was performed. The support structure has been accepted by the MI engineering group, however, more detailed stress analysis needs to be performed on the wall extension to ensure that it can handle the beam detector in the test area. Lastly, the detector itself has also been verified to handle 2 atm of air within the RF cavity body, as it met all of the necessary requirements based on stress analysis calculations.

Acknowledgements

I would like to thank my mentor, Katsuya Yonehara, for his guidance and support throughout this project. I would also like to thank everyone in the Lee Teng Internship program, especially Peter Garbincius, for allowing me to have this valuable opportunity.

References

[1]K. Yonehara. 1-MW Target and Beam Detector Upgrade Project. Fermilab.

[2]T. Roberts. G4Beamline User's Guide 3.04. Muons, Inc.

[3]K. Yonehara. "First Beam Test of RF Beam Detector." Gas RF Detector Meeting. Fermilab. 2/20/2018.

[4]R. Beardmore. Loaded Flat Plates. Retrieved from http://www.roymech.co.uk/Useful_Tables/Mechanics/Plates.html

[5]K. Yonehara. Stress Analysis of High-Pressure Test Vessel (Draft v1.4). Fermilab.